*Inorg. Chem.* **2005**, *44*, 1309–1318


# Cadmium Amido Alkoxide and Alkoxide Precursors for the Synthesis of Nanocrystalline CdE (E = S, Se, Te)

**Timothy J. Boyle,* Scott D. Bunge, Todd M. Alam, Gregory P. Holland, Thomas J. Headley, and Gabriel Avilucea**

*Advanced Materials Laboratory, Sandia National Laboratories, 1001 University Boulevard SE, Albuquerque, New Mexico 87105*

Received October 22, 2004

The synthesis and characterization of a family of alternative precursors for the production of CdE nanoparticles (E = S, Se, and Te) is reported. The reaction of $Cd(NR_2)_2$ where $NR_2 = N(SiMe_3)_2$ with *n* HOR led to the isolation of the following: $n = 1$ $[Cd(\mu\text{-}OCH_2CMe_3)(NR_2)(py)]_2$ (**1**, py = pyridine), $Cd[(\mu\text{-}OC_6H_3(Me)_2\text{-}2,6)_2Cd(NR_2)(py)]_2$ (**2**), $[Cd(\mu\text{-}OC_6H_3(CHMe_2)_2\text{-}2,6)(NR_2)(py)]_2$ (**3**), $[Cd(\mu\text{-}OC_6H_3(CMe_3)_2\text{-}2,6)(NR_2)(py)]_2$ (**4**), $[Cd(\mu\text{-}OC_6H_2(NH_2)_3\text{-}2,4,6)(NR_2)\text{-}(py)]_2$ (**5**), and $n = 2$ $[Cd(\mu\text{-}OC_6H_3(Me)_2\text{-}2,6)(OC_6H_3(Me)_2\text{-}2,6)(py)_2]_2$ (**6**), and $[Cd(\mu\text{-}OC_6H_3(CMe_3)_2\text{-}2,6)(OC_6H_3\text{-}(CMe_3)_2\text{-}2,6)(THF)]_2$ (**7**). For all but **2**, the X-ray crystal structures were solved as discrete dinuclear units bridged by alkoxide ligands and either terminal $-NR_2$ or $-OR$ ligands depending on the stoichiometry of the initial reaction. For **2**, a trinuclear species was isolated using four $\mu$-OR and two terminal $-NR_2$ ligands. The coordination of the Cd metal center varied from 3 to 5 where the higher coordination numbers were achieved by binding Lewis basic solvents for the less sterically demanding ligands. These complexes were further characterized in solution by $^1H$, $^{13}C$, and $^{113}Cd$ NMR along with solid-state $^{113}Cd$ NMR spectroscopy. The utility of these complexes as "alternative precursors" for the controlled preparation of nanocrystalline CdS, CdSe, and CdTe was explored. To synthesize CdE nanocrystals, select species from this family of compounds were individually heated in a coordinating solvent (trioctylphosphine oxide) and then injected with the appropriate chalcogenide stock solution. Transmission electron spectroscopy and UV–vis spectroscopy were used to characterize the resultant particles.

## Introduction

Nanomaterials are of increased interest based on the promise of novel physical behavior related to surface phenomena that dominate on this length scale. Examples of this would include photoluminescent quantum dots (i.e., CdE where E = S, Se, Te) that demonstrate different color emissions based on the size of the nanoparticle. The strong size and shape dependent optical properties of these materials have led to their use in optoelectronic devices[1−3] and as biological tags.[4−8] As the application of CdE materials grows, more flexible precursors will be necessary to generate tailor-made, high-quality quantum dots with specific properties. It was recently reported that the toxic, pyrophoric, and unstable $Me_2Cd$ typically used to synthesize CdE materials, could be replaced by "green precursors" such as the acetate, oxide, and carbonate derivatives with significant improvements in the final CdE materials.[9] Metalorganic species, such as alkoxides or amides, may yield even greater improvements due to the control that can be introduced by the readily accessible varied ligand sets.

Currently there is a dearth of structural information involving cadmium alkoxides ($Cd(OR)_2$).[10−14] This can be

* To whom correspondence should be addressed. E-mail: tjboyle@Sandia.gov. Phone: (505) 272-7625. Fax: (505) 272-7336.

(1) Romanov, S. G.; Chigrin, D. N.; Torres, C. M. S.; Gaponik, N.; Eychmuller, A.; Rogach, A. L. *Phys. Rev. E: Stat., Nonlinear, Soft Matter Phys.* **2004**, *69*, 46606.
(2) Gaponik, N.; Eychmuller, A.; Rogach, A. L.; Solovyev, V. G.; Torres, C. M. S.; Romanov, S. G. *J. Appl. Phys.* **2004**, *95*, 1029.
(3) Yu, A. M.; Meiser, F.; Cassagneau, T.; Caruso, F. *Nano Lett.* **2004**, *4*, 177.
(4) Pinaud, F.; King, D.; Moore, H. P.; Weiss, S. *J. Am. Chem. Soc.* **2004**, *126*, 6115.
(5) Nisman, R.; Dellaire, G.; Ren, Y.; Li, R.; Bazett-Jones, D. P. *J. Histochem. Cytochem.* **2004**, *52*, 13.
(6) Mansson, A.; Sundberg, M.; Balaz, M.; Bunk, R.; Nicholls, I. A.; Omling, P.; Tagerud, S.; Montelius, L. *Biochem. Biophys. Res. Commun.* **2004**, *314*, 529.
(7) Sukhanova, A.; Devy, M.; Venteo, L.; Kaplan, H.; Artemyev, M.; Oleinikov, V.; Klinov, D.; Pluot, M.; Cohen, J. H. M.; Nabiev, I. *Anal. Biochem.* **2004**, *324*, 60.
(8) Derfus, A. M.; Chan, W. C. W.; Bhatia, S. N. *Nano Lett.* **2004**, *4*, 11.
(9) Qu, L. H.; Peng, Z. A.; Peng, X. G. *Nano Lett.* **2001**, *1*, 333.

10.1021/ic0485155 CCC: $30.25 
Published on Web 01/25/2005

rationalized by the relative thermal instability of the combination of a soft metal with a hard alkoxy ligand. If properly controlled, however, this characteristic instability can be exploited to fine-tune nanocrystal CdE production. To do this in a meaningful manner, a family of closely related precursors must be synthesized and systematically processed to generate materials under identical conditions. We have previously shown how this approach worked for ZnO nanoparticles wherein we synthesized a family of mono-, di-, tetra-, and heptanuclear zinc alkyl alkoxide precursors that were then systematically converted to ZnO nanomaterials using 1-methyl imidazole and water.[15] From this study, it was found that the structure of the Zn−O central core of the precursors play a pivotal role in the aspect ratio of the resultant nanorods.

Using a similar approach, we undertook the synthesis and characterization of a series of cadmium amido alkoxides [Cd(NR$_2$)(OR)], and cadmium(II) alkoxide [Cd(OR)$_2$] compounds which were then used to generate quantum dots. Since the potentially useful precursor, cadmium bistrimethylsilylamide [Cd(NR$_2$)$_2$] derivative, is a liquid at room temperature, it was omitted from consideration in this study. The alcohols investigated ranged from *neo*-pentanol (H−OCH$_2$CMe$_3$, HONep), 2,6-di-methyl phenol (H−OC$_6$H$_3$(Me)$_2$-2,6, H-DMP), 2,6-di-*iso*-propyl phenol (H−OC$_6$H$_3$(CHMe$_2$)$_2$-2,6, H-DIP), 2,6-di-*tert*-butyl phenol (H−OC$_6$H$_3$(CMe$_3$)$_2$-2,6, H-DBP), and 2,4,6-tris(dimethyl amino methyl phenol (H−OC$_6$H$_2$(CH$_2$NMe$_2$)$_3$-2,4,6, H-TMAP). This family of compounds was synthesized through the alkoxy amide exchange shown in eq 1 in toluene (tol), tetrahydrofuran (THF) and/or pyridine (py).

$$\mathrm{Cd(NR_2)_2} + \underset{n=1,2}{n\mathrm{HOR}} \rightarrow \mathrm{Cd(NR_2)_{2-n}(OR)_n(solv)} \quad (1)$$

The following heteroligated compounds were identified as [Cd($\mu$-ONep)(NR$_2$)(py)]$_2$ (**1**); Cd[($\mu$-DMP)$_2$Cd(NR$_2$)(py)]$_2$ (**2**); [(py)$_2$(DMP)Cd($\mu$-DMP)$_2$Cd(NR$_2$)(py)] (**2a**); [Cd($\mu$-OAr)(NR$_2$)]$_2$, OAr = DIP (**3**), DBP (**4**), and TMAP (**5**). Plots of **1**, **2**, **2a**, **4**, and **5** are shown in Figures 1−5, respectively. Note that a plot of **3** can be found in the Supporting Information. The homoligated compounds were identified as [Cd($\mu$-DMP)(DMP)(py)$_2$]$_2$ (**6**) and [Cd($\mu$-DIP)(DIP)(THF)]$_2$ (**7**). Plots of **6** and **7** are shown in Figures 6 and 7, respectively. This report is an effort to shed light into the structural chemistry of cadmium aryloxides and examine their potential use as precursors for semiconductor nanocrystals.

## Experimental Section

All compounds described below were handled with rigorous exclusion of air and water using standard Schlenk line and glovebox techniques. Diethyl ether, THF, and py were stored under argon and used as received (Aldrich) in sure seal bottles. The following chemicals were used as received (Aldrich): CdBr$_2$, Li(NR$_2$), H-ONep, H-DMP, H-DIP, H-DBP, H-TMAP, Se (−100 mesh, 99.5+ %), Te (−40 mesh, 99.997%), S(SiMe$_3$)$_2$, technical grade (90%) trioctylphosphine oxide (TOPO), 99% TOPO, and technical grade trioctylphosphine (TOP, 90%). Tetradecylphosphonic acid (TDPA) and octadecylphosphonic acid (ODPA) were purchased

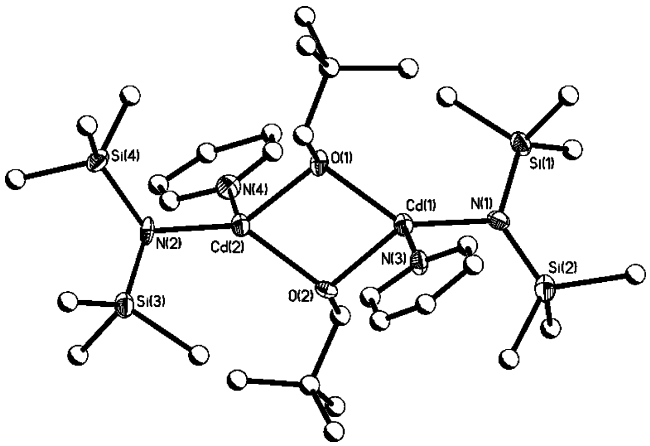


**Figure 1.** Structure plot of **1**. Thermal ellipsoids of heavy atoms drawn at 30% level. Carbon atoms are drawn as ball-and-stick for clarity.

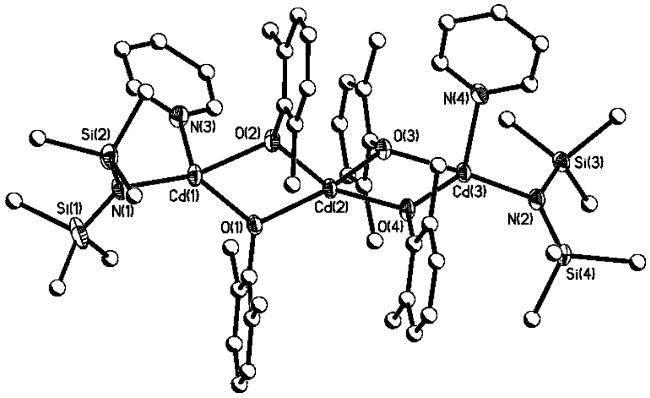


**Figure 2.** Structure plot of **2**. Thermal ellipsoids of heavy atoms drawn at 30% level. Carbon atoms are drawn as ball-and-stick for clarity.

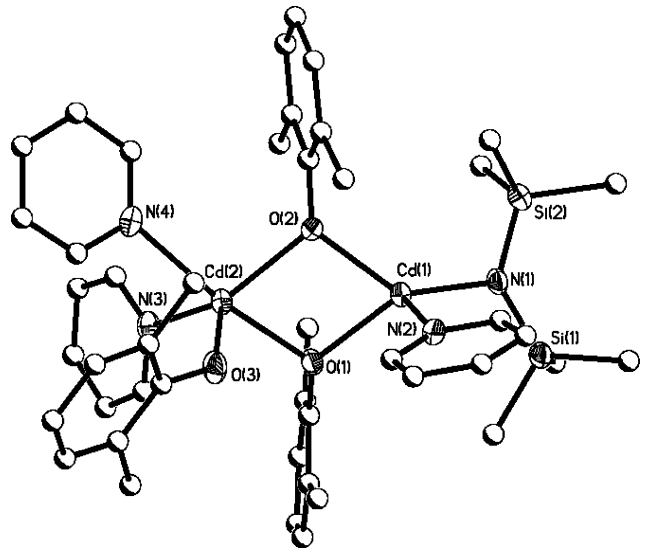


**Figure 3.** Structure plot of **2a**. Thermal ellipsoids of heavy atoms drawn at 30% level. Carbon atoms are drawn as ball-and-stick for clarity.

(10) Darensbourg, D. J.; Niezgoda, S. A.; Draper, J. D.; Reibenspies, J. H. *J. Am. Chem. Soc.* **1998**, *120*, 4690.
(11) Darensbourg, D. J.; Niezgoda, S. A.; Reibenspies, J. H.; Draper, J. D. *Inorg. Chem.* **1997**, *36*, 5686.
(12) Boulmaaz, S.; Papiernik, R.; Hubert-Pfalzgraf, L. G.; Vaissermann, J.; Daran, J.-C. *Polyhedron* **1992**, *11*, 1331.
(13) Herrmann, W. A.; Huber, N. W.; Priermeier, T. *Angew. Chem., Int. Ed. Engl.* **1994**, *33*, 105.
(14) Goel, S. C.; Chiang, M. Y.; Buhro, W. E. *J. Am. Chem. Soc.* **1990**, *112*, 6724.
(15) Boyle, T. J.; Bunge, S. D.; Andrews, N. L.; Matzen, L. E.; Sieg, K.; Rodriguez, M. A.; Headley, T. J. *Chem. Mater.* **2004**, 16, 3279.

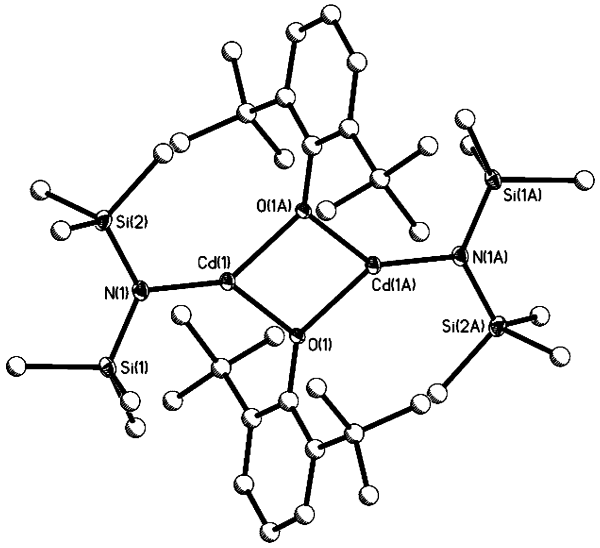


**Figure 4.** Structure plot of **4**. Thermal ellipsoids of heavy atoms drawn at 30% level. Carbon atoms are drawn as ball-and-stick for clairity.

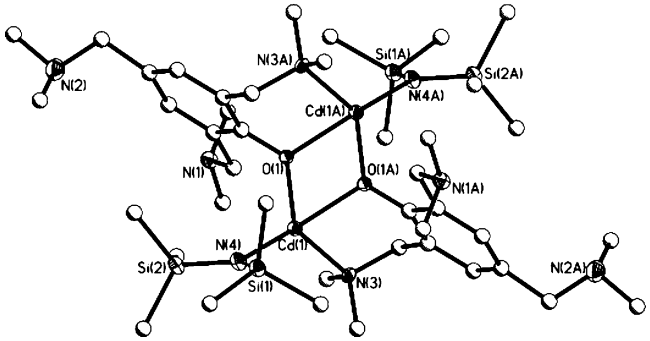


**Figure 5.** Structure plot of **5**. Thermal ellipsoids of heavy atoms drawn at 30% level. Carbon atoms are drawn as ball-and-stick for clarity.

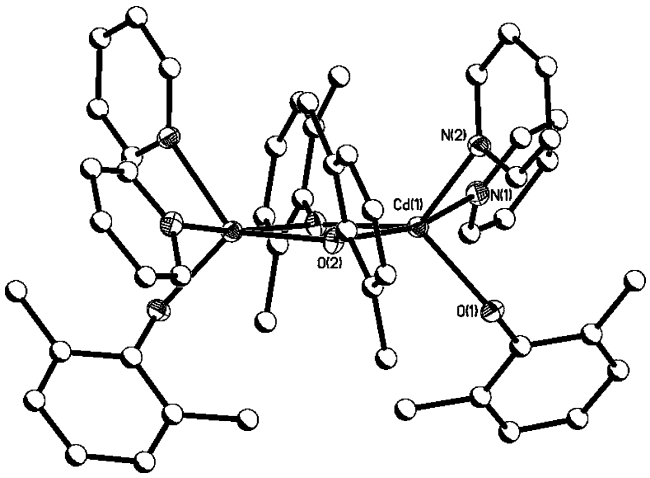


**Figure 6.** Structure plot of **6**. Thermal ellipsoids of heavy atoms drawn at 30% level. Carbon atoms are drawn as ball-and-stick for clarity.

from Alfa Aesar. Methanol (99.9%) and acetone (99.7%) were purchased from Fisher and used as received. $Cd(NR_2)_2$ was synthesized with minor modification from literature reports using $CdBr_2$ and 2 equiv of $Li(NR_2)$.[16]

FT-IR data were obtained on a Bruker Vector 22 Instrument using KBr pellets under an atmosphere of flowing nitrogen.

(16) Burger, H.; Sawodny, W.; Wannagat, U. *J. Organomet. Chem.* **1965**, *3*, 113.

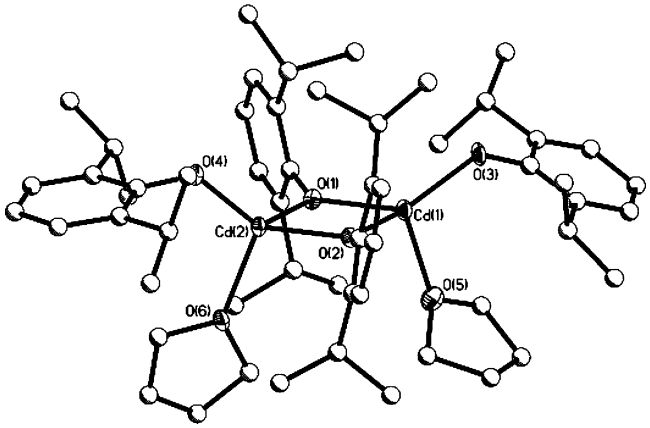


**Figure 7.** Structure plot of **7**. Thermal ellipsoids of heavy atoms drawn at 30% level. Carbon atoms are drawn as ball-and-stick for clarity.

Elemental analysis was performed on a Perkin-Elmer 2400 CHN-S/O elemental analyzer. All NMR samples were prepared from dried crystalline materials that were handled and stored under an argon atmosphere and redissolved in the appropriate deuterated solvent (toluene-$d_8$) at saturated solution concentrations. All solution spectra were obtained on a Bruker DRX400 spectrometer at 399.8 and 100.5 MHz for $^1$H and $^{13}$C experiments, respectively. A 5 mm broadband probe was used for all experiments. $^1$H NMR spectra were obtained using a direct single pulse excitation, with a 10 s recycle delay and 8 scan average. The $^{13}$Cd NMR spectra were obtained using a WALTZ-16 composite pulse $^1$H decoupling, a 5 s recycle delay, and a $\pi/4$ pulse excitation.

Rotors of dry crystalline materials of **1**−**4** were packed under an inert atmosphere, and $^{113}$Cd NMR spectra were collected. The chemical shift was referenced against a 1.0 M (aq) $Cd(ClO_4)_2$ solution (0.0 ppm) using solid $CdCl_2$ as a secondary standard (183 ppm).[17] The $^{113}$Cd solid-state spectra were collected under magic angle spinning (MAS) conditions at a rotor spinning frequency of 5 kHz. A single $\pi/2$ pulse of 2 $\mu$s was applied with a 60 s recycle delay, and 2048 scan averages were obtained for each sample. Multiple MAS frequencies were attempted to discern the isotropic chemical shift. The spinning sideband manifold was fit with the DMFIT software package[18] to extract both the chemical shift anisotropy (CSA) and asymmetry parameter ($\eta$).

**General Synthesis.** The 1 or 2 equiv of the appropriate alcohol were slowly added to a vial containing $Cd(NR_2)_2$ in toluene to generate the respective hetero- or homoligated species. Upon addition, the initial yellow tinged reaction mixture remained clear and was allowed to stir for 12 h. After this time, a precipitate formed for most of the samples. For these reactions, pyridine was added and the reaction mixture was warmed until clear. Crystals were grown either by transferring the mixture to a freezer (−37 °C) or allowing them to sit uncapped in the glovebox until crystals formed. Yields were not optimized. *Note! Extreme care must be taken in the handling and storage of cadmium containing compounds, as well as the subsequent waste due to the extreme toxicity associated with this metal.*

**[Cd($\mu$-ONep)($NR_2$)(py)]$_2$ (1).** $Cd(NR_2)_2$ (1.00 g, 2.31 mmol) and HONep (0.203 g, 2.31 mmol) in ∼5 mL toluene were used. Yield 46.5% (0.47 g). FTIR (KBr, cm$^{-1}$) 2950(s), 2932(s), 284(s), 2778-(w), 2741(w), 2706(w), 147(m), 1461(m), 1395(w), 1363(m), 1334-

(17) Sakida, S.; Shojiya, M.; Kawamoto, Y. *Solid State Commun.* **2000**, *115*, 553.

(18) Massiot, D.; Fayon, F.; Capron, M.; King, I.; LeCalvé, S.; Alonso, B.; Durand, J.-O.; Bujoli, B.; Gan, Z.; Hoatson, G. *Magn. Reson. Chem.* **2002**, *40*, 70.

(w), 1261(m), 1188(m), 1076(s), 1056(s), 1018(s), 958(w), 937(w), 920(w), 901(w), 832(m), 756(m,sh), 679(s), 588(m), 529(sh,m). $^{113}$Cd(88.7 MHz, tol-$d_8$) $\delta$ 356 (1 Cd), 241 (2.5 Cd), 138, 137 (0.4 Cd). Anal. Calcd for $C_{32}H_{68}Cd_2N_4O_2Si_4$: C, 43.77; H, 7.81; N, 6.38. Found: C, 43.67; H, 8.09; N, 5.99.

**Cd[($\mu$-DMP)$_2$Cd(NR$_2$)(py)]$_2$ (2).** $Cd(NR_2)_2$ (1.00 g, 2.31 mmol) and H-DMP (0.283 g, 2.31 mmol) in ~ 5 mL toluene were used. Yield 38.0% (0.380 g). FTIR (KBr, cm$^{-1}$) 3067(w), 3036(w), 2958-(s br), 1061(m), 1591(m), 1475(s), 1466(m), 1460(m), 1446(m), 1422(m), 1265(s), 1231(m), 1215(w), 1092(m), 1068(m), 933(m), 877(m, sh), 845(s), 753(m), 701(m). $^{113}$Cd(88.7 MHz, tol-$d_8$) $\delta$ 213.8 (2 Cd), 90.0 (1 Cd). Anal. Calcd for $C_{54}H_{82}Cd_3N_4O_4Si_4$: C, 49.86, 6.35 H, 4.31 N. Found 49.46 C, 6.73 H, 4.56 N.

**[Cd($\mu$-DIP)(NR$_2$)]$_2$ (3).** $Cd(NR_2)_2$ (1.00 g, 2.31 mmol) and H-DIP (0.412 g, 2.31 mmol) in ~ 5 mL toluene were used. Yield 59.6% (0.62 g). FTIR (KBr, cm$^{-1}$) 3061(w), 3025(w), 2960(s), 2928(m sh), 2871(m), 1460(m), 1430(s), 1383(m), 1360(m), 1319 (m), 1258(s), 1248(s), 1184(s), 1107(m), 989(m), 932(w), 873(m), 832(s), 756(s), 678(m), 618(m), 569(m), 537(w), 464(w). $^{113}$Cd-(88.7 MHz, tol-$d_8$) $\delta$ 250.0 (1 Cd), 157.5 (3.6 Cd), 139.1 (0.5 Cd), 9.0 (0.3 Cd). Anal. Calcd for $C_{18}H_{35}CdNOSi_2$: C, 48.03; H, 7.84; N, 3.11. Found C, 48.07; H, 7.79; N, 2.95.

**[Cd($\mu$-DBP)(NR$_2$)]$_2$ (4).** $Cd(NR_2)_2$ (1.00 g, 2.31 mmol) and H-DBP (0.477 g, 2.31 mmol) in ~5 mL toluene were used. Yield 81.1% (0.90 g). FTIR (KBr, cm$^{-1}$) 3094(w), 3072(w), 2958(s), 2919(m, sh), 2875(m, sh) 1466(w), 1459(w), 1405(s), 1385(m), 1260(s), 1250(s), 1211(s), 1190(s), 1120(m), 961(s), 872(s), 845-(m), 825(m), 789(m), 756(m), 721(w), 699(m), 633(w). $^{113}$Cd (88.7 MHz, tol-$d_8$) $\delta$ 142.1 (1 Cd). Anal. Calcd for $C_{40}H_{78}Cd_2N_2O_2Si_4$: C, 50.24; H, 8.12; N, 2.93. Found: C, 50.12; H, 8.00; N, 2.86.

**[Cd($\mu$-TMAP)(NR$_2$)]$_2$ (5).** $Cd(NR_2)_2$ (0.48 g, 1.1 mmol) and H-TMAP (0.29 g, 1.1 mmol) in ~5-mL were used. Yield 59.4% (0.35 g). FTIR (Nujol, cm$^{-1}$) 2963(s), 2905(w), 1447(w), 1414-(w), 118(s), 1007(s), 876(m), 823(s), 787(s), 705(w), 686(w), 443-(m). $^1$H NMR (399.8 MHz, $CDCl_3$) $\delta$ 7.08, 6.96 (1.0H, s, $OC_6H_2(CH_2N(CH_3)_2)_3$), 3.65, 3.31 (6.0H, s, $OC_6H_2(CH_2N(CH_3)_2)_3$), 2.27, 2.16 (18.0H, s, $OC_6H_2(CH_2N(CH_3)_2)_3$), 0.06 (18.0H, s, $N(Si(CH_3)_3)_2$). $^{13}$C{$^1$H} NMR (100.5 MHz, tol-$d_8$) $\delta$ 168.3, 153.5, 131.8, 127.3 ($OC_6H_2(CH_2N(CH_3)_2)_3$), 71.6, 62.3 ($OC_6H_2(CH_2N(CH_3)_2)_3$), 47.5, 45.8 ($OC_6H_2(CH_2N(CH_3)_2)_3$). $^{29}$Si{$^1$H} NMR (tol-$d_8$) $\delta$ −4.51. $^{113}$Cd NMR (py-$d_5$) $\delta$ 213.8. Anal. Calcd for $C_{42}Cd_2H_{88}N_8O_2Si_4$: C, 46.91; H, 8.19; N 10.42. Found: C, 46.82; H, 7.86; N 9.43.

**[Cd($\mu$-DMP)(DMP)(py)$_2$]$_2$ (6).** $Cd(NR_2)_2$ (0.48 g, 1.1 mmol) and H-DMP (0.27 g, 2.2 mmol) in ~5 mL py were used. Yield 51.0% (0.20 g). FTIR (KBR, cm$^{-1}$) 2975(s), 2952(m), 2905(w), 1445(m), 1414(m), 1247(s), 1156(s), 989(s), 883(s), 777(m), 754-(m), 707(m), 662(wm), 450(m). $^1$H NMR (399.8 MHz, py-$d_5$) $\delta$ 7.13 (2.0H, d, $OC_6H_3(CH_3)_2$)), 6.65 (1.0H, m, $OC_6H_3(CH_3)_2$)), 2.50 (6.0H, s, $OC_6H_3(CH_3)_2$)). $^{13}$C{$^1$H} NMR (100.5 MHz, py-$d_5$) $\delta$ 168.3, 129.1, 126.6, 124.5, 114.3 ($OC_6H_3(CH_3)_2$), 19.1 ($OC_6H_3-(CH_3)_2$)). $^{113}$Cd NMR (py-$d_5$) 105.2. Anal. Calcd for $C_{52}Cd_2-H_{56}N_4O_4$: C, 60.83; H, 5.46; N, 5.46. Found: C, 61.04; H, 5.53; N, 5.19.

**[Cd($\mu$-DIP)(DIP)(THF)]$_2$ (7).** $Cd(NR_2)_2$ (0.48 g, 1.1 mmol) and H-DIP (0.40 g, 2.2 mmol) in ~5 mL THF were used. Yield 48.7% (0.25 g). FTIR (Nujol, cm$^{-1}$) 2979(s), 2949(m), 1588(w), 1484-(w), 1415(s), 1244(s), 1172(s), 981(s), 887(m), 774(m), 753(m), 684(m), 661(w), 450(m); $^1$H NMR (399.8 MHz, THF-$d_8$) $\delta$ 6.82 (2.0H, d, $OC_6H_3(CH(CH_3)_2)_2$), 6.46 (1.0H, t, $OC_6H_3Me_2$), 3.38 (2.0H, m, $OC_6H_3(CH(CH_3)_2)_2$), 1.16 (12.0H, d, $OC_6H_3(CH(CH_3)_2)_2$). $^{13}$C{$^1$H} NMR (100.5 MHz, THF-$d_8$) $\delta$ 167.8, 131.7, 129.8, 123.1 ($OC_6H_3(CH(CH_3)_2)_2$), 28.0 ($OC_6H_3(CH(CH_3)_2)_2$), 23.8 ($OC_6H_3(CH-(CH_3)_2)_2$). $^{113}$Cd NMR (THF-$d_8$): $\delta$ 0.944. Anal. Calcd for $C_{56}-Cd_2H_{84}O_6$: C, 62.34; H, 7.79. Found: C, 61.91; H, 7.55.

**General Synthesis of CdE Nanoparticles.** The general synthesis follows for the CdE materials produced using the various Cd precursors. Under flowing argon in a 250 mL three-neck flask equipped with a septum, a thermometer adapter, and a gas adapter, TOPO, TDPA, or ODPA, and the desired Cd precursor were mixed. The Cd solution was then heated to 320 °C with stirring. In a glovebox, a chalcogenide stock solution was prepared by mixing TOP, anhydrous toluene (~0.1 g), and the desired chalcogenide: (i) $S(SiMe_3)_2$, (ii) Se, or (iii) Te. The chalcogenide stock solution was drawn into a syringe (3 mL) in the glovebox, transferred to the Schlenk line, and then rapidly injected (~1.0 s) into the heated Cd solution. After the appropriate time (15 s to 2 h), the reaction vessel was placed into a boiling water bath. Once the reaction mixture reached ~60 °C, the reaction was quenched via the addition of a previously prepared 50:50 methanol/acetone solution.

**(i) CdS Nanoparticles.** Compound **2** or **7** (0.38 mmol), TOPO 90% (3.8 g, 9.0 mmol), $S(SiMe_3)_2$ (0.10 g, 0.60 mmol), and TOP (2.0 g, 5.0 mmol) were used in the previously described synthesis. The reaction time was 4 min.

**(ii) CdSe Nanoparticles.** Compound **3** or **7** (0.39 mmol), TOPO 90% (3.8 g, 9.0 mmol), TDPA (0.22 g, 7.0 mmol), Se (0.041 g, 0.50 mmol), and TOP (2.0 g, 5.0 mmol) were used in the previously described synthesis. The reaction time was 2 min.

**(iii) CdTe Nanoparticles.** Compound **4** or **7** (0.80 mmol), TOPO 90%(3.2 g, 7.6 mmol), ODPA (0.80 g, 0.30 mmol), Te (0.034 g, 0.30 mmol), and TOP (2.0 g, 5.0 mmol) were used in the previously described synthesis. The reaction time was 5 min.

**General X-ray Crystal Structure Information.**[17] Each crystal was mounted onto a thin glass fiber from a pool of Fluorolube and immediately placed under a liquid $N_2$ stream, on a Bruker AXS diffractometer. The radiation used was graphite monochromatized Mo K$\alpha$ radiation ($\lambda$ = 0.7107 Å). The lattice parameters were optimized from a least-squares calculation on carefully centered reflections. Lattice determination and data collection were carried out using SMART Version 5.054 software. Data reduction was performed using SAINT Version 6.01 software. Structure refinement was performed using XSHELL 3.0 software. The data were corrected for absorption using the SADABS program within the SAINT software package.

Each structure was solved using direct methods that yielded the heavy atoms, along with a number of the C, N, and O atoms. Subsequent Fourier synthesis yielded the remaining atom positions. The hydrogen atoms were fixed in positions of ideal geometry and refined within the XSHELL software. The idealized hydrogen atoms had their isotropic temperature factors fixed at 1.2 or 1.5 times the equivalent isotropic $U$ of the C atoms to which they were bonded. The final refinement of each compound included anisotropic thermal parameters on all non-hydrogen atoms. Additional information concerning the data collection and final structural solutions of **1**−**7** can be found in the Supporting Information. Table 1 lists the data collection parameters for **1**−**7**, respectively.

**Optical Characterization.** UV−vis absorption spectra were collected at room temperature on a Varian Carey 400 spectrophotometer. Each aliquot was quenched directly in a UV cell containing toluene. The spectra were collected from 800 to 300 nm with a scan rate of 0.5 nm per minute.

**Transmission Electron Microscopy (TEM).** An aliquot of the desired solution was placed directly onto a carbon coated copper TEM grid (300 mesh) purchased from Electron Microscopy Sciences. The aliquot was then allowed to dry overnight. The

**Table 1.** Data Collection Parameters for **1**−**7**

| | **1** | **2** | **2a** | **3** | **4** | **5** | **6** | **7** |
|---|---|---|---|---|---|---|---|---|
| chemical formula | $C_{32}H_{68}N_4O_2Si_4$ | $C_{108}H_{164}N_8O_8Si_8$ | $C_{45}H_{60}Cd_2N_4O_3Si_2$ | $C_{72}H_{140}Cd_4N_4O_4Si_8$ | $C_{40}H_{78}Cd_2N_2O_2Si_4$ | $C_{42}H_{88}Cd_2N_8O_2Si_4$ | $C_{52}H_{56}Cd_2N_4O_4$ | $C_{56}H_{84}Cd_2O_6$ |
| fw | 878.06 | 2601.59 | 985.95 | 1800.20 | 956.20 | 1074.36 | 1025.81 | 1078.03 |
| temp (K) | 203(2) | 203(2) | 203(2) | 203(2) | 168(2) | 168(2) | 168(2) | 168(2) |
| space group | triclinic | monoclinic | monoclinic | monoclinic | triclinic | monoclinic | monoclinic | orthorhombic |
| | *P*1 | $P2_1/c$ | $P2_1$ | $P2_1/c$ | *P*1 | $P2_1/n$ | *C*2/*c* | $P2_12_12_1$ |
| *a* (Å) | 9.5720(10) | 33.733(4) | 9.9973(4) | 17.051(2) | 10.078(2) | 13.871(2) | 21.819(7) | 16.026(5) |
| *b* (Å) | 10.1847(10) | 17.768(2) | 13.6501(6) | 17.567(2) | 11.736(3) | 13.832(2) | 9.497(3) | 16.579(5) |
| *c* (Å) | 12.5815(12) | 23.015(3) | 17.4569(8) | 31.225(4) | 11.869(3) | 14.788(2) | 22.736(7) | 20.494(6) |
| α (deg) | 98.7510(10) | | | | 66.838(3) | | | |
| *β* (deg) | 109.9070(10) | 98.717(2) | 94.7970(10) | 90.139(3) | 88.463(3) | 102.302(3) | 99.469(5) | |
| *γ* (deg) | 98.741(12) | | | | 70.341(3) | | | |
| *V* (Å$^3$) | 1112.09(19) | 13635(3) | 2373.90(18) | 9353(2) | 1206.4(4) | 2772.1(8) | 4647(3) | 5445(3) |
| *Z* | 1 | 4 | 2 | 4 | 1 | 2 | 4 | 4 |
| $D_{calcd}$(mg/m$^3$) | 1.311 | 1.267 | 1.379 | 1.278 | 1.316 | 1.287 | 1.466 | 1.315 |
| $\mu$(Mo Kα) (mm$^{-1}$) | 1.093 | 1.036 | 0.987 | 1.040 | 1.012 | 0.892 | 0.964 | 1.040 |
| R1[a] (%) (all data) | 2.96 (3.44) | 6.77 (9.79) | 2.83 (3.14) | 12.33 (15.09) | 1.72 (1.81) | 4.43 (8.11) | 3.33 (5.37) | 5.01 (9.49) |
| wR2[b] (%) (all data) | 6.45 (6.80) | 21.13 (23.64) | 5.88 (6.12) | 26.43 (27.62) | 4.43 (4.49) | 8.25 (9.40) | 6.44 (7.00) | 8.71 (10.88) |

[a] $R1 = \sum||F_o| - |F_c||/\sum|F_o| \times 100$. [b] $wR2 = [\sum w(F_o^2 - F_c^2)^2/\sum(w|F_o|^2)^2]^{1/2} \times 100$.

resultant particles were studied using a Philips CM 30 TEM operating at 300 kV accelerating voltage.

## Results and Discussion

A series of structurally characterized heteroleptic "Cd(OR)($NR_2$)" complexes and homoleptic "Cd$(OR)_2$" were evaluated as precursors to CdE nanocrystals to determine precursor structural effects on the final materials morphologies. No reports of structurally characterized heteroligated "Cd(OR)($NR_2$)" were available in the literature, and until recently, the existence of $Cd(OR)_2$ as discrete, structurally characterized, molecular species was limited to a few homo- and heterometallic compounds.[10−14] The synthesis, characterization, and properties of all precursors and the resultant CdE nanomaterials are discussed below.

**Synthesis.** The reaction shown in eq 1 was followed for the synthesis of the family of "Cd($NR_2$)(OR)" compounds. For each sample, the $Cd(NR_2)_2$ precursor was dissolved in tol and allowed to react overnight with the desired HOR. Except for the DBP derivative, a precipitate formed which would not redissolve even upon heating. Pyridine was added and the reaction was heated until the reaction mixture turned clear. Crystals were grown by allowing the reaction mixtures to cool and slowly evaporate or cooling the reaction mixture to −37 °C overnight. Plots of **1**, **2**, and **2a** are shown in Figures 1−3, respectively, where **1** and **2** were found to possess coordinated py solvent molecules. An additional off stoichiometric species was also isolated for **2** and crystallographically characterized as $Cd_2(\mu\text{-DMP})_2(DMP)(NR_2)(py)_3$ (**2a**) (Figure 3). This was generated when a slight excess of H-DMP was added to the reaction mixture. No further attempts were made to synthesize this compound or fully characterize it; however, its structure demonstrates the various constructs that are available to tailor the properties of the final CdE nanoparticles generated in this system. The DIP (**3**, Supporting Information) and DBP derivative (**4**, Figure 4) were easily crystallized from toluene. The same structure was also solved for crystals of **4** grown from py. The TMAP derivative (**5**), also grown from toluene, is shown in Figure 5.

Cadmium aryloxide derivatives (**6**, **7**) were synthesized in good yield by treatment of $Cd(NR_2)_2$ with 2 equiv of an appropriate phenol (eq 2). Selected coordinating Lewis basic solvents were chosen to assist in the dissolution and crystallization of these compounds. The $n = 2$ reaction (eq 1) with DMP in py yielded **6**, whereas with DIP in THF, **7** was isolated. Structure plots of **6** and **7** are shown in Figures 6 and 7, respectively.

**Crystal Structures.** Single-crystal X-ray diffraction studies were undertaken to determine the structural aspects of these compounds prior to formation of CdE nanoparticles. For **1** (Figure 1), each Cd metal center adopts a distorted tetrahedral (Td) geometry using a terminal $NR_2$, two $\mu$-ONep, and a coordinated py solvent molecule. A trinuclear species was isolated for the DMP derivative **2** (Figure 2). The central Cd was found to adopt a Td arrangement using four $\mu$-DMP. The Td bound terminal Cd atoms are additionally bound by a terminal $NR_2$ and a py molecule. An additional structure was isolated for a reaction mixture that had a slight excess of H-DMP as **2a**, shown in Figure 3. The Cd metal centers are again Td and possess two $\mu$-DMP. One of the Cd metal centers binds a DMP ligand and two py molecules, whereas the other Cd binds the $NR_2$ and one py molecule.

Both **3** (Supporting Information) and **4** (Figure 4) have similar arrangements where each of the Cd metal centers adopt a trigonal planar arrangement using one terminal $NR_2$ and two $\mu$-OAr. Neither compound, when isolated from py, showed any coordinated solvent. The increased steric bulk of the *ortho* substituents prevents further coordination by the Lewis basic solvent.

A plot of **5** reveals that the polydentate TMAP-ligated compound is dinuclear and solvent-free in the solid state (Figure 5). Each Td-bound Cd atom is coordinated to one terminal amido ligand, intramolecularly coordinated to the nitrogen atom of the dimethylamino substituent, and is linked to the other Cd atom by two symmetrical bridging TMAP ligands. The amido aspect of the ligand prevents further coordination by any solvent molecules.

Investigation of the full alkoxides led to the isolation of compounds **6** and **7**, shown in Figures 6 and 7, respectively.

The solid-state dinuclear structures are similar to the amido alkoxy species, wherein each trigonal-bipyramidal (TBP) Cd atom of **6** bridges to the other Cd atom via two $\mu$-DMP ligands. The TBP coordination is completed by the addition of one terminal DMP and two py solvent molecules. The Td Cd atoms of **7** are bound two $\mu$-DIP ligands as well as one terminal DIP ligand and one molecule of THF.

The bond distances and angles of the "$Cd(NR_2)(OR)$" species **1**−**7** are consistent with those of the previously reported Cd−(OR)[10−14] and −$(NR_2)$[19−23] species. The terminal aryloxide ligands of **6** and **7** notably exhibit a small Cd−O−Ar angle, demonstrating the absence of $\pi$ -donation from the aryl ring, a feature typically found present in early-transition metal aryloxide compounds.[24,25]

**Bulk Properties.** To establish that the crystal structures of **1**−**7** are representative of the bulk material, Fourier transformed infrared (FTIR) spectroscopy, elemental analysis (EA), and additional analytical information were collected. The data garnered are discussed in the following paragraphs.

The FTIR spectra of **1**−**7** show no OH peaks around 3000 $cm^{-1}$ which is consistent with full exchange. For **1**−**5**, the normally strong $M-NR_2$ amide stretches present around 1400−1450 $cm^{-1}$ are weaker due to the dominating presence of the alkyl and solvent stretches, in comparison to the other family members due to the dominating presence of the alkyl and solvent stretches. For **2**, the $NR_2$ resonances are weaker in comparison to the other members of this family. This is consistent with the extended trinuclear structure observed in the solid state. For the M−O bonds there should be a stretch present between 800 and 400 $cm^{-1}$. Each sample also had a stretch around 755 $cm^{-1}$ that was tentatively assigned to Cd−O. For **1**, another very broad and strong stretch associated with py is observed that is not present or is present at lower levels for the other species. The EAs of the bulk powders for **1**−**7** were found to be consistent with the solid-state structure. This is surprising for a number of the compounds reported, since molecules with coordinated solvents often yield inconsistent elemental analyses.[26] In addition, amido species are often volatile and too reactive to obtain meaningful analysis.

**NMR Studies: Solution Behavior.** $^{13}C$ and $^{1}H$ NMR spectra were collected for **1**−**7**; however, the data obtained were not informative with respect to the nuclearity of the complexes in solution. The appropriate sets of ligand resonances were observed for each sample but definitive statements concerning the solution structure were not discernible. Therefore, $^{113}Cd$ NMR spectra were collected for each compound and are metrically listed in Table 2. As indicated by previous studies, the variation of the $^{113}Cd$ chemical shifts is very complex:[10,11,27] the ligand set and the coordination number (CN) dramatically affect both the isotropic $^{113}Cd$ chemical shift and shielding anisotropy. In addition rapid exchange of ligands along with coordination by Lewis basic solvents is possible in solution and further complicates the position of the chemical shift.[28]

**Table 2.** $^{113}Cd$ NMR Data for **1**−**7**

| compd | nuclearity Cd CN solv | $\delta$ solution -state $^{113}Cd$ (integration) | $\delta$ solid-state $^{113}Cd$ (integration) |
|---|---|---|---|
| **1** | dinuclear, 4 py | 356(1), 241(2.5), 138, 137(0.4) | + 304, 302, 300 |
| **2** | trinuclear, 4 py | 213.8(2), 90.0(1) | |
| **3** | dinuclear, 3 tol | 250.0(1), 157.5(3.6), 139.1(0.5), 9.0(0.3) | + 202, 200, 198, 196, 192 |
| **4** | dinuclear, 3 tol | 142.1(1) | + 179, 176, 173 |
| **5** | dinuclear, 4 tol | 213.8 | |
| **6** | dinuclear, 4 py | 105.2 | |
| **7** | dinuclear, 4 THF | 0.944 | |

In general, for the same ligand type an increase in the Cd CN results in a decrease in the observed $^{113}Cd$ isotropic chemical shift.[28] A fully oxygen coordinated Cd species (either 5 or 6 coordinated) would be predicted to have a $^{113}Cd$ NMR chemical shift between −10 and +235 ppm.[27−29] Introduction of sulfur in place of oxygen atoms increases the observed $^{113}Cd$ chemical shift on the order of +300 to +400 ppm. In comparison, a similar substitution of nitrogen for oxygen atoms increases the observed $^{113}Cd$ chemical shift by approximately +100 to +200 ppm. For example, the cadmium(II) maleate dehydrate has $^{113}Cd$ chemical shifts at $\delta$ −7 and +12 ppm, while the heterometalic alkoxide, $[Cd\{Zr_2(OPr^i)_9\}]$ ($OPr^i$ = $OCHMe_2$), has a $^{113}Cd$ shift of +67 ppm (CN = 5: all O atoms), $CdNb_2(O_2CCH_3)_2(OPr^i)_{10}$ (CN = 5: all O atoms) of +34 ppm,[30] and $[\{Cd(OPr^i)_3\}Ba\{Zr_2(OPr^i)_9\}]_2$ (CN = 4: all O atoms) of +235 ppm.[29] In comparison, the octahedrally coordinated Cd with two N atoms in $Na_2Cd(EDTA)$ (CN = 6: two N and four O atoms) has a $^{113}Cd$ shift of approximately +110 to +95 ppm.[28] These shifts and predicted changes can be used to understand the spectra observed in the characterization of **1**−**7**.

For compound **1**, the $^{113}Cd$ NMR shifts in solution ($\delta$ = +356 ppm) and in the solid-state ($\delta$ approximately +302 ppm) correspond to the retention of the dinuclear solid-state structure in solution (CN = 4: two N and two O atoms). The appearance of additional $^{113}Cd$ resonance in solution reveals that there is considerable rearrangement of the molecule in solution. This dynamic ligand behavior may statistically generate up to at least 8 types of Cd species (4: 0, 3:1, 2:2, 1:3, 0:4 $NR_2$/OR; for 4 dimers and 4 monomers). Compound **2a** represents an example of the structure that

(19) Bashall, A.; Beswick, M. A.; Harmer, C. N.; McPartlin, M.; Paver, M. A.; Wright, D. S. *J. Chem. Soc., Dalton Trans.* **1998**, 517.
(20) Beswick, M. A.; Cromhout, N. L.; Harmer, C. N.; Palmer, J. S.; Raithby, P. R.; Steiner, A.; Verhorevoort, K. L.; Wright, D. S. *Chem. Commun.* **1997**, 583.
(21) Cummins, C. C.; Schrock, R. R.; Davis, W. M. *Organometallics* **1991**, *10*, 3781.
(22) Bailey, P. J.; Mitchell, L. A.; Raithby, P. R.; Rennie, M. A.; Verhorevoort, K.; Wright, D. S. *Chem. Commun.* **1996**, 1351.
(23) Just, O.; Gaul, D. A.; Rees, W. S. *Polyhedron* **2001**, *20*, 815.
(24) Kerschner, J. L.; Fanwick, P. E.; Rothwell, I. P.; Huffman, J. C. *Inorg. Chem.* **1989**, *28*, 780.
(25) Coffindaffer, T. W.; Steffy, B. D.; Rothwell, I. P.; Folting, K.; Huffman, J. C.; Streib, W. E. *J. Am. Chem. Soc.* **1989**, *111*, 4742.
(26) Boyle, T.; Alam, T.; Mechenbier, E.; Scott, B.; Ziller, J. *Inorg. Chem.* **1997**, *36*, 3293.
(27) Summers, M. F. *Coord. Chem. Rev.* **1988**, *86*, 43.
(28) Wasylishen, R. E.; Fyfe, C. A. High-Resolution NMR of Solids. In *Annual Reports on NMR Spectroscopy*; Webb, G. A., Ed.; Academic Press: New York, 1982; Vol. 12; p 1.
(29) Veith, M.; Mathur, S.; Hunch, V. *J. Am. Chem. Soc.* **1996**, *118*, 903.
(30) Boulmaaz, S.; Papiernik, R.; Hubert-Pfalzgraf, L. G.; Septe, B.; Vassermann, J. *J. Mater. Chem.* **1997**, *7*, 2053.

could form in solution for a 1:3 arrangement. The observation of resonances between +241 and +137 ppm suggests that either an increase in the CN in solution or a substitution of oxygen-coordinating ligands in place of nitrogen-coordinating ligands is occurring.

The trinuclear compound **2** shows resonances at $\delta = +213$ and +90. The down field chemical shift is consistent with CN = 5 and suggests coordination by N atoms such as that observed for the terminal Cd metal centers in **2**. The resonance at +90 suggests a fully O coordinated environment such as that observed for the central Cd atom in compound **2**.

For **3**, the $^{113}$Cd NMR chemical shift in solution ($\delta$ = +250 ppm) and in the solid-state ($\delta$ approximately +200 ppm) is assigned to the trigonally coordinated Cd species (CN = 3: one N and two O atoms). Literature values for trigonal coordinated Cd species are limited, but the chemical shift observed for **3** is higher than the +77 ppm $^{113}$Cd NMR chemical shift reported for the Cd environment with trigonal oxygen coordination in cadmium phenoxides,[31] but is closer to a proposed related pyridine adduct of cadmium phenoxide.[32] The change from an oxygen donating ligand to a nitrogen donating ligand is expected to increase the observed $^{113}$Cd chemical shift by ~100 ppm, as noted above. The additional $^{113}$Cd resonances observed in solution suggest significant changes in the coordination environment with dissolution for this compound.

Due to the simplicity of the observed single $^{113}$Cd peaks recorded for **5**−**7**, it is difficult to state whether the structure is retained in solution or not. It appears, based on the chemical shift, that **5** retains its dinuclear Td environment; however, the chemical shifts for **6** and **7** do not agree. Due to the large sterically bulky ligands, it is assumed that these species are monomeric in solution with significant shifts upfield due to change in CN.

Solid-state $^{113}$Cd NMR data were also collected on select compounds in an effort to discern additional information about the local bonding environments of these molecules. Figure 8 shows the $^{113}$Cd MAS NMR spectra of **2**, **3**, and **4**. Very large spinning sideband manifolds that span hundreds of ppm resulting from chemical shift anisotropy (CSA) were observed. The observed CSAs were 960 ppm for **4**, 987 ppm for **3**, and 660 ppm for **1**. From previous solid-state $^{113}$Cd NMR investigation of sulfur-coordinated Cd species, it was demonstrated that the magnitude of the CSA anisotropy reflects the range of bonding distances associated with Cd, while the CSA asymmetry reflects the local site symmetries.[33,34] In addition, $^{113}$Cd isotropic resonances of similar chemical shift were experimentally observed (see inset of Figure 8) for each of these compounds. Due to the extreme sensitivity of $^{113}$Cd NMR chemical shifts to local environments, small differences in the isotropic chemical shifts were attributed to small differences in local crystal packing.

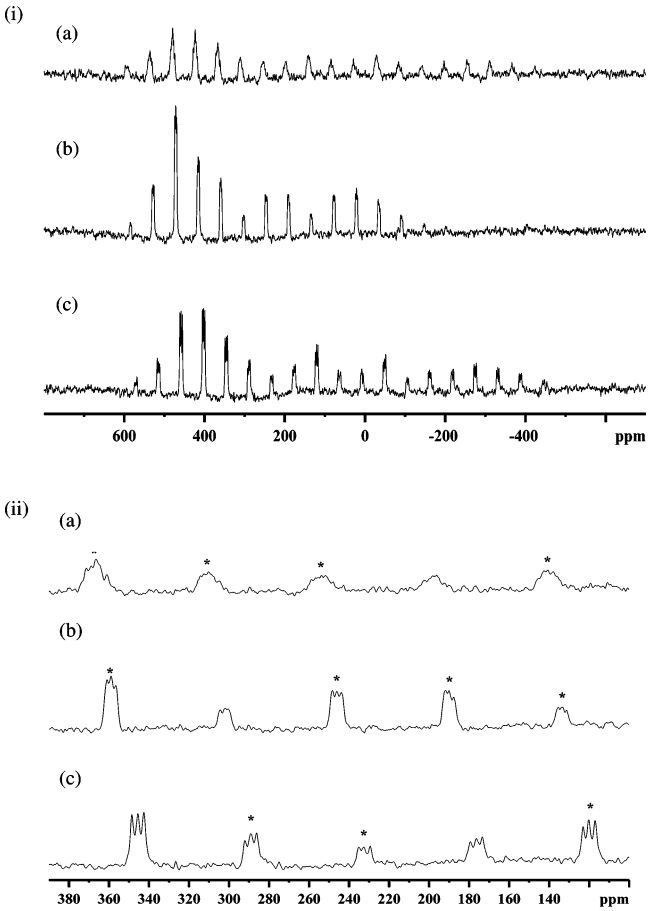


**Figure 8.** Solid-state $^{113}$Cd MAS NMR spectra of (i) (a) **3**, (b) **1**, and (c) **4** and (ii) expansion of the isotropic region of the $^{113}$Cd MAS NMR spectra of (a) **3**, (b) **1**, and (c) **4**.

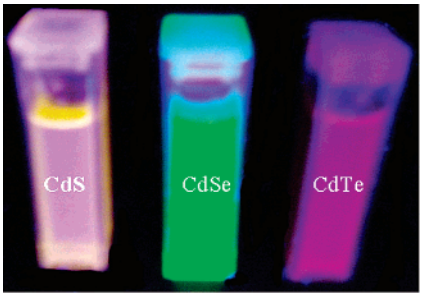


**Figure 9.** Irradiated CdE solutions (a) **2**, E = S, (b) **3**, E = Se, and (c) **4**, E = Te.

Attempts to draw a correlation between the major peaks in the solid and in the solution phase did not yield conclusive evidence for peak assignments concerning nuclearity of the structures. For **1** and **3**, the solid-state resonances of the dinuclear species fall between the two major peaks observed in solution. For **4**, the solid-state resonance is 30 ppm less than the solution resonance. If this trend is true, then the major peaks observed for **1**, **3**, and **5** are consistent with the dinuclear species, whereas **6** and **7** would have to represent mononuclear species. This implies the structures observed in the solid state are retained in solution.

(31) Darensbourg, D. J.; Wildeson, J. R.; Lewis, S. J.; Yarbrough, J. C. *J. Am. Chem. Soc.* **2002**, *124*, 7075.
(32) Darensbourg, D. J.; Niezgoda, S. A.; Draper, J. D.; Reibenspies, J. H. *J. Am. Chem. Soc.* **1998**, *120*, 4690.
(33) Lee, G. S. H.; Fisher, K. J.; Vassallo, A. M.; Hanna, J. V.; Dance, I. G. *Inorg. Chem.* **1993**, *32*, 2.
(34) Murphy, P. D.; Stevens, W. C.; Cheung, T. T. P.; Lacelle, S.; Gerstein, B. C.; Kurtz, D. M., Jr. *J. Am. Chem. Soc.* **1981**, *103*, 4400.

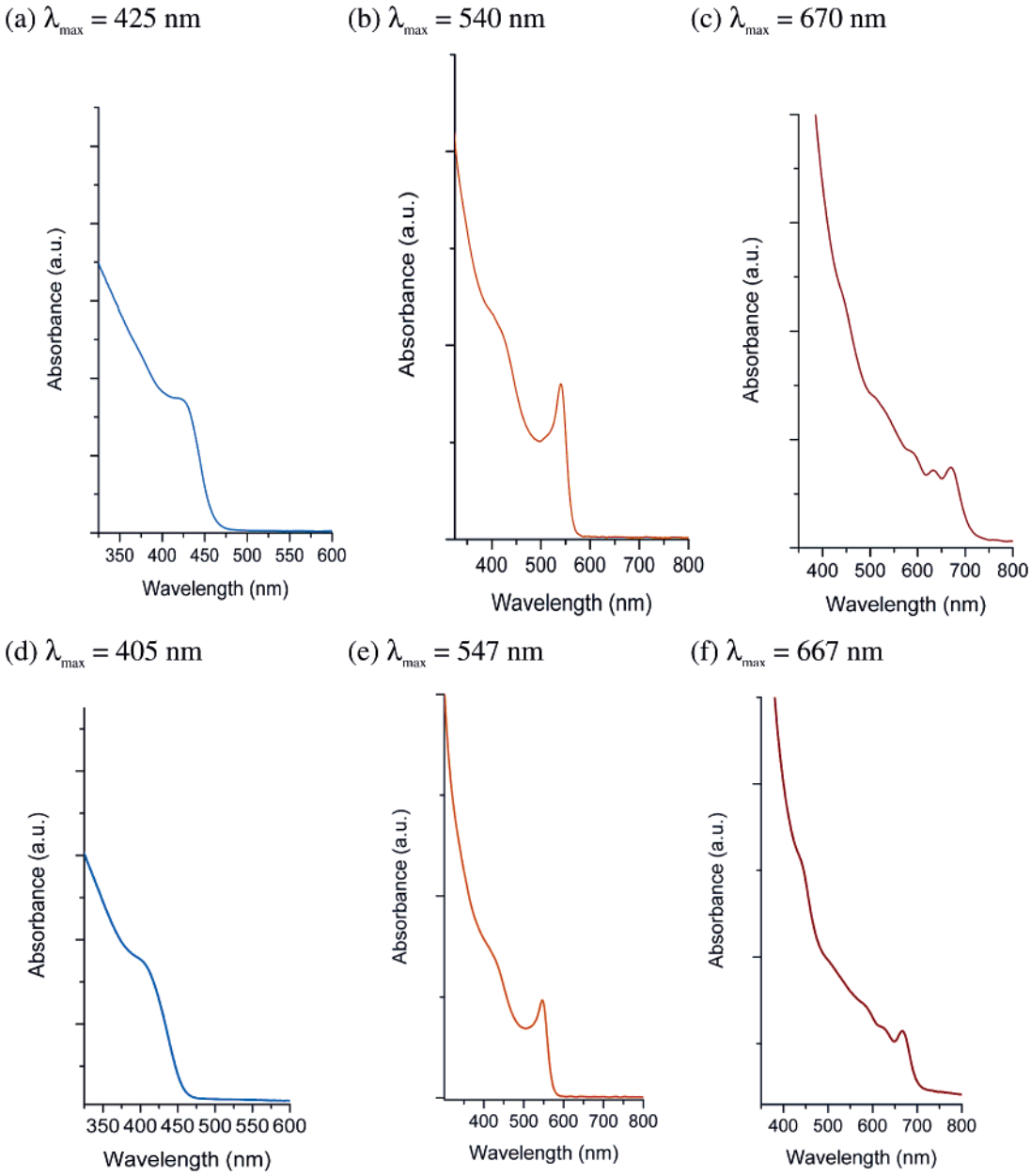


**Figure 10.** UV−vis spectra for CdE materials generated from (a) **2**, E = S, (b) **3**, E = Se, (c) **4**, E = Te, (d) **7**, E = S, (e) **7**, E = Se, and (f) **7**, E = Te.

**Nanoparticle Synthesis.** While existing reports indicate that the choice of precursors has relatively little effect on the final CdE nanoparticles' morphology, the presence of a free amine and alcohol (which would be expected to form upon decomposition of **2**−**7**) may have a larger effect than decomposition products from the other Cd precursors investigated. Further, the lower decomposition temperatures expected for the compounds reported here in comparison to the previously reported "green" precursors should allow for altered growth patterns. CdE nanoparticles, synthesized from **2**−**7**, were prepared by slight modification to a method recently investigated by Peng and co-workers (i.e., CdS and CdSe) and also Alivisatos and co-workers (i.e., CdTe).[35,36] Experimentally, TOPO, ODPA, or TDPA and the cadmium precursor were heated until a transparent solution resulted. A chalcogenide solution was then injected, and the growth temperature was set to 320 °C. The progress of crystal growth for each CdE was monitored by UV−vis spectroscopy and TEM. For all of the reactions, the ratio of cadmium precursor to surfactants, the moles of chalcogenide injected, and the temperature of the reaction over a 2 h time period were kept constant. Under these conditions, it was found that the oxide (CdO) and acetate ($Cd(OAc)_2$) derivatives yielded nanoparticles of similar sizes and shapes.

A survey of the cadmium chalcogenides was performed with these novel precursors. A different precursor was used for each synthesis to determine the general utility of these compounds in the preparation of CdE nanoparticles. Figure 9 illustrates that all the particles generated were high quality

(35) Peng, Z. A.; Peng, X. G. *J. Am. Chem. Soc.* **2001**, *123*, 183.
(36) Manna, L.; Milliron, D. J.; Meisel, A.; Scher, E. C.; Alivisatos, A. P. *Nat. Mater.* **2003**, *2*, 382.

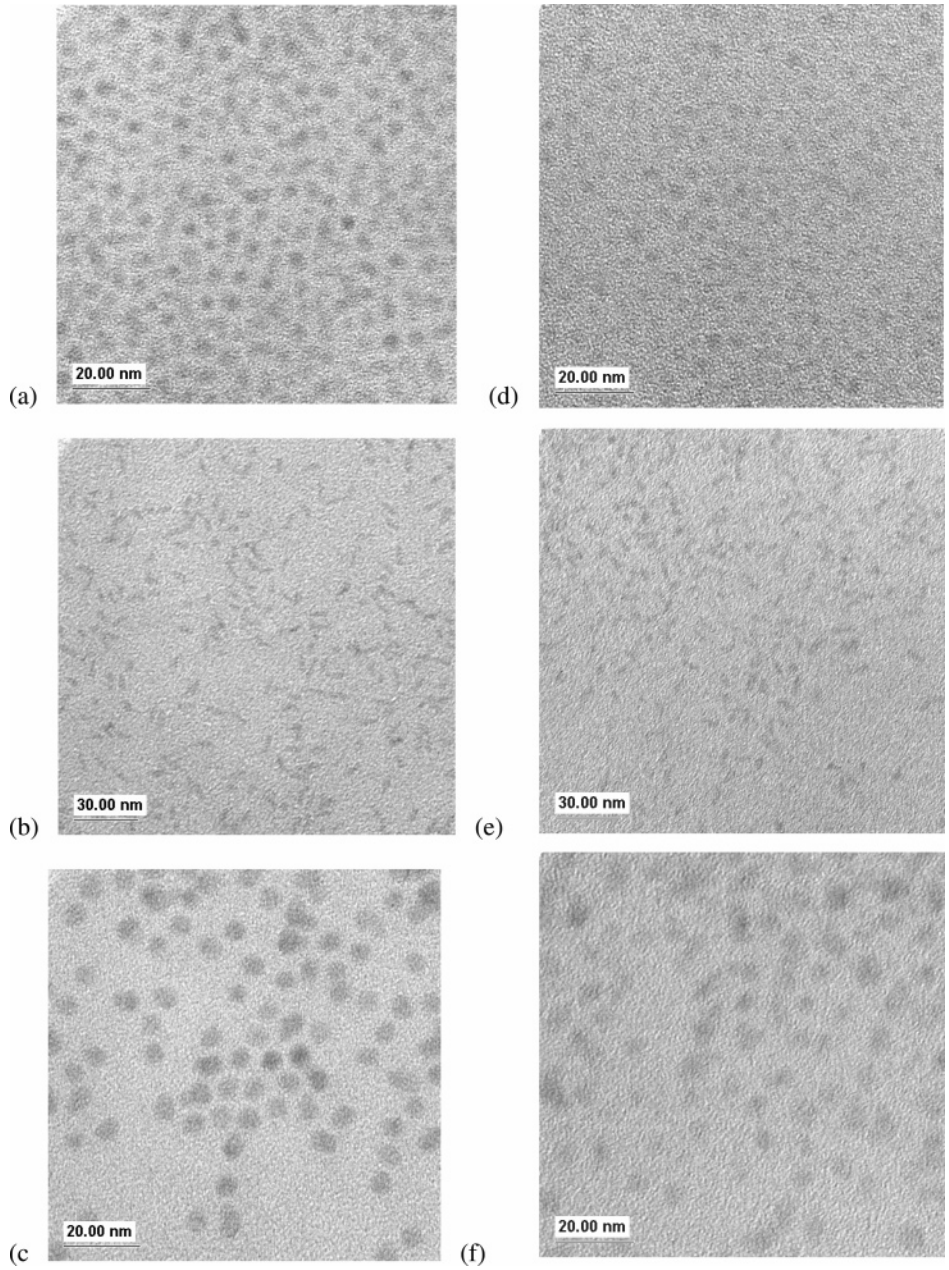


**Figure 11.** TEM images of CdE from (a) **2**, E = S, (b) **3**, E = Se, (c) **4**, E = Te, (d) **5**, E = S, (e) **6**, E = Se, and (f) **7**, E = Te.

luminescent materials. The UV−vis spectra and TEM images are shown in Figures 10 and 11, respectively. The high quality of the material isolated indicates the potential utility of these precursors in controlling the various physical properties of CdE materials.

**Cadmium Sulfide.** The reaction systems for both compounds remained pale yellow during the synthesis of the nanocrystals. The UV−vis spectra of the CdS nanoparticles from the heteroligated (**2**) and homoligated (**5**) species are shown in Figure 10a,d. These spectra revealed an absorption at $\lambda_{max} = 425$ and 400 nm, for **2** and **5**, respectively. These emissions are consistent with the literature reports on TOP capped CdS nanocrystals of 4−5 nm in size.[37] TEM images (Figure 11a,d) confirm the expected 4−5 nm sized nanoparticles with little variation in spherical morphology for either precursor (Figure 11a,d). From this study, the amine or alcohol generated upon decomposition of either the homo or heteroligated species was unable to facilitate anisotropic wurtzite growth of CdS under the reaction conditions presented, thus spherical shapes were obtained for both samples.

**Cadmium Selenide.** Under identical synthetic conditions to CdS, the cadmium reaction mixture changed from light yellow to wine red upon injection of the Se/TOP stock solution. The UV−vis spectra of the CdSe from **3** or **6** (Figure 10b,e) show a $\lambda_{max} = 540$ nm for the heteroligated and $\lambda_{max} = 547$ nm for the homoligated species. The UV−vis spectra indicate 3 nm CdSe were produced. The TEM images (Figure 11b,d) show ill-defined rods are formed from both precursors. The width are consistent with the 3 nm

(37) Bunge, S. D.; Krueger, K. M.; Boyle, T. J.; Rodriguez, M. A.; Headley, T. J.; Colvin, V. L. *J. Mater. Chem.* **2003**, *13*, 1705.

observed in the UV−vis spectrum (the width is the only dimension will possess an emission for this shaped material). As previously described, the presence of TDPA preferentially poisons the 001 face.[37] Surprisingly, in comparison to the use of CdO or $Cd(OAc)_2$ as precursors, well-defined nanorods with uniform aspect ratios were not generated from this synthesis when the same reaction conditions are used. This clearly demonstrates that the precursors have a significant effect on the growth and morphology of the final CdE materials.

**Cadmium Telluride.** With respect to the synthesis of CdTe nanocrystals, the reaction mixture changed from colorless to dark brown-red upon injection of the Te stock solution at 320 °C. The UV−vis spectra show a $\lambda_{max} = 670$ and 680 nm (Figure 10c,f) for **4** and **7**, respectively, which are consistent with CdTe nanocrystals 6−7 nm in size. TEM images confirm the spherical nature and size of the CdTe nanoparticles (Figure 11c,f). The CdTe morphology generated under these synthetic conditions is unusual since a tetrapod morphology is typically observed.[36] Apparently compounds **4** and **7** via decomposition generate conditions that inhibit the wurtzite growth of the tetrapodal arms.

## Summary and Conclusions

A family of alternative "$Cd(OR)(NR_2)$" and "$Cd(OR)_2$" precursors were synthesized and structurally characterized for production of CdE materials. The change in steric bulk around the metal center had little effect on the structure of the majority of species isolated since most were isolated as a dinuclear species. This is unusual since additional coordination sites were available as evidenced by the ability of some Cd metal centers to bind solvent molecules. The presence of additional coordination sites is important because the homoleptic amides are very sensitive to atmospheric water and the homoleptic alkoxides, while more stable, can easily oligomerize reducing their utility. With the mixed ligand set, not only can we fine-tune the various properties of interest, we can also use these species to form more complex heteroleptic alkoxide species in a controlled manner. Solution-state and solid-state NMR data show the bulk materials are consistent with the solid-state structures; however, a great deal of fluxtionality was noted on the basis of $^{113}Cd$ NMR data.

Using these specialty precursors, we systematically generated a series of CdE materials under identical conditions to explore the effect the hetero- and homoligand sets have on the final morphology of the CdE material. It was found that (i) CdS spheres, (ii) CdSe rods, and (iii) CdTe spheres were isolated for both homo- and heteroligated species. These morphologies were different from those noted in the literature using "green precursors" under identical synthesis conditions. Therefore, the morphological changes must be related to the influence of the decomposition byproducts of the starting precursors, poisoning and promoting different growth planes. Additional work in understanding how to further garner control over the growth of final materials is underway based on the fundamental information learned in this study.

**Acknowledgment.** For support of this research, the authors would like to thank the Office of Basic Energy Sciences of the Department of Energy and the United States Department of Energy. Sandia is a multiprogram laboratory operated by Sandia Corporation, a Lockheed Martin Company, for the United States Department of Energy under contract DE-AC04-94AL85000.

**Supporting Information Available:** Crystallographic data in CIF format and additional figure. This material is available free of charge via the Internet at http://pubs.acs.org.

IC0485155